View metadata, citation and similar papers at core.ac.uk
brought to you by CORE
provided by Repository@USM

DESIGN AND MODELING OF DIELECTRIC RESONATOR ANTENNA ARRAY USING NEW FEEDING METHOD OVER A SHORT ENDED MICROSTRIP

By

YAZEED M.A QASAYMEH

Thesis submitted in fulfillment of the requirements for the degree of Doctor of Philosophy

July 2013

DESIGN AND MODELING OF DIELECTRIC RESONATOR ANTENNA ARRAY USING NEW FEEDING METHOD OVER A SHORT ENDED MICROSTRIP

YAZEED M.A QASAYMEH

UNIVERSITI SAINS MALAYSIA
2013

DEDICATION

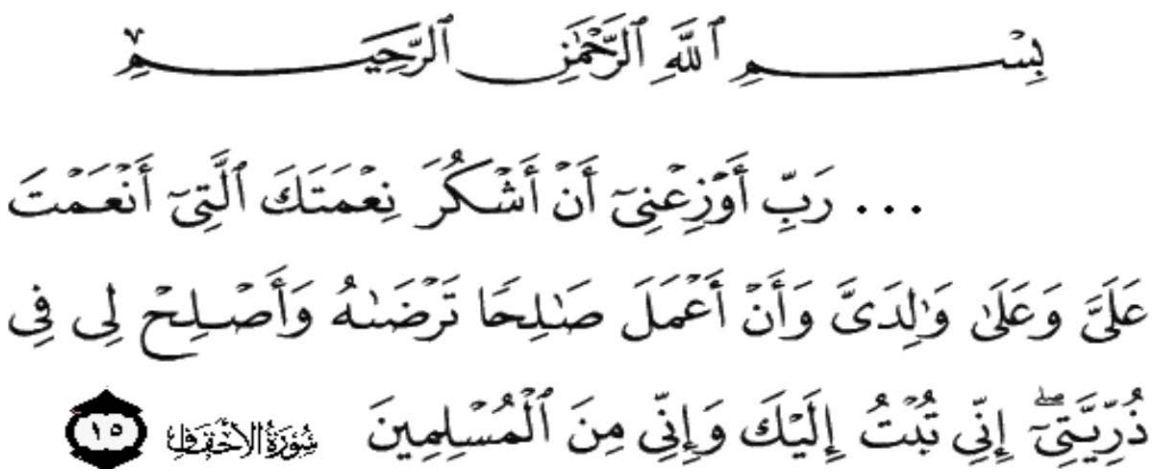

Praise be to Allah, the most gracious and the most merciful. Without his blessing and guidance my accomplishments would never have been possible.

My father Mohd Akram and my mother Yusra Mohd for their patience and support for all these years

My supervisor Assoc. Prof. Dr. Mohd Fadzil Ain and my co-supervisor Prof .Hj Zainal Ariffin bin Ahmad

My fiancée who always light up for me.

ACKNOWLEDGMENT

I would like to express my thanks and appreciation to my supervisors, Associate Professor Dr. Mohd Fadzil Ain and Prof Zainal Arifin Ahmad for their encouragement and support during the duration of my study. Their advice and constructive criticism have been of tremendous bedrock of this work. They have demonstrated immensely the capacity to device a far reaching research project. Their guidance and consistent encouragement had allowed me to complete this work successfully. I am extremely impressed with their instructions, advice and generosity.

To my mind, Dr Fadzil was more than just a supervisor. He is a father, and has demonstrated consistently so, and more particularly when I have challenges. In times of need, he treated me as one of his own sons. I am very impressed with the way he manage his research group with careful planning and much patience. I am truly grateful and considered it a rare privilege to have you as my supervisor.

Further thanks to my research team members namely; Azman Zakaria, Mohd Arrif Othman, Khairul Anuar, Seyi Olokede, Roslina bt Hussin, Syazana Basyirah, Samiyah Umill Hakim, Mutasem Khasawneh, Ihsan Zubir , Zulhelmi and Nik Akmar for their help, support, and friendship during my dark times. Also, I would like to thank Mr. Latip Hamid, Mr. Ellias, Mr. Zuber, Mr. Hisham and Mrs Zamira for their help during my stay in USM

Finally, I would like to acknowledge the financial support of the FRGS grant under project number 203/PELECT/6071183, USM Short Term Grant under project no. 304/ PBAHAN/6039035 and the USM Research University (RU) Grant under project numbers .1001/PELECT/814117 and 1001/PELECT/854004.

TABLE OF CONTENTS

DEDICATION ii

ACKNOWLEDGMENT iii

TABLE OF CONTENTS iv

LIST OF TABLES. xi

LIST OF FIGURES……..……..xii

LIST OF SYMBOLS xviii

LIST OF ABBREVIATIONS xxi

ABSTRAK xxiii

ABSTRACT xxv

CHAPTER ONE

INTRODUCTION 1

1.1 Background 1

1.2 Problem Statement 2

1.3 Objectives 3

1.4 Research Scope and Limitations 4

1.5 Thesis Contribution 6

1.6 Thesis Outline 7

CHAPTER TWO

LITERATURE REVIEW 9

2.1 Introduction……..…….……9

2.1.1 Dielectric Resonator Antenna 10

2.1.2 Features 12

2.1.3 Rectangular DRA 13

2.1.3.1 Field Modes..... 13

2.1.3.2 Dielectric Waveguide Model for Rectangular DRAs 17

2.1.3.3 Resonant Frequency 20

2.1.3.4 Q-Factor 20

2.1.3.5 Radiation Model..... 21

2.1.3.6 Radiation Efficiency of a Rectangular DRA..... 22

2.1.3.7 Rectangular Dielectric Resonator Dimensions 23

2.1.4 Substrate Parameters Effects on Antenna 24

2.1.5 Microstrip Aperture Coupling..... 27

2.1.6 Microstrip Stub Extension and the Guided Wavelength..... 29

2.2 Related Research…….…..……..…32

2.2.1 Fed Mechanisms for Linear DRA Array..... 32

2.2.1.1 Microstrip-Coupled Linear DRA Arrays 32

2.2.1.1.1 Microstrip Series Fed Line..... 32

2.2.1.1.2 Microstrip Parallel Network……..……..33

2.2.1.1.3 Microstrip Branch Line Fed..... 36

2.2.1.2 Probe-Coupled Linear DRA Arrays with Microstrip Corporate Feed 37

2.2.1.3 Dielectric Image Guide Feed ..... .40

2.2.2 Circularly Polarized DRA Arrays…….…….……...41

2.2.2.1 Circularly Polarized DRAs with Single Point Feed..... ….46

2.2.3 Broadband Dielectric Resonator Antenna Arrays..... .49

2.2.3.1 Bandwidth Enhancement for Simple Shaped DRAs..... .51

2.3 Summary……...56

CHAPTER THREE

METHODOLOGY..... .57

3.1 Introduction..... 57

3.2 Proposed DRA Arrays 60

3.2.1 Principle of Feeding Mechanism 60

3.2.2 Design of Wideband Array using Notched Rectangular Dielectric Resonator 62

3.2.3 Design of Circularly Polarized Array using Rectangular Dielectric Resonator 63

3.2.4 Design of Circularly Polarized Wideband Array using Notched Rectangular Dielectric Resonator..... 66

3.3 Proposed Approximate Input Impedance Model of DRA Microstrip Slot Coupled ..... .67

3.3.1 Impedance of Microstrip..... 69

3.3.2 Impedance of the Slot 71

3.3.3 Impedance of the Dielectric Resonator..... 72

3.3.4 Equivalent Circuit of Microstrip Slot Coupled Dielectric Resonator Antenna Array 75

3.4 Antenna Resonator Fabrication 77

3.4.1 Dielectric Material Preparation……...77

3.4.2 Mixing 78

3.4.3 Calcination 78

3.4.4 Pressing 79

3.4.5 Sintering 80

3.5 Dielectric Properties Characterization 87

3.5.1 Field Emission Scanning Electron Microscopy 81

3.5.2 X-Ray Diffraction 81

3.5.3 Dielectric Properties at High Frequency 82

3.6 Modeling of the DRA Array Input Impedance in ADS 83

3.7 Antenna Simulation Using CST Microwave Studio 84

3.7.1 Setting of Dielectric Substrate 84

3.7.2 Setting of Microstrip Feeder 84

3.7.3 Defining of Waveguide Port 84

3.7.4 Defining of Boundary Conditions 84

3.7.5 Far-Field Monitor 85

3.7.6 Transient Solver 85

3.8 Measurements of the Antenna 86

3.8.1 S-Parameter Measurement 86

3.8.2 Antenna Radiation Pattern Measurement..... 86

3.8.3 Antenna Gain Measurement..... 88

3.8.4 Antenna Axial Ratio..... 90

3.9 Summary……92

CHAPTER FOUR

RESULTS AND DISCUSSIONS..... 92

4.1 Introduction..... 92

4.2 Dielectric Materials Analysis..... 92

4.2.1 XRD Analysis..... 92

4.2.1.1 CCTO.. ……92

4.2.1.2 ZST……..... 94

4.2.2 FESEM Analysis..... 94

4.2.2.1 CCTO.. ……94

4.2.2.2 ZST……..... 95

4.2.3 Dielectric Constant Determination..... 96

4.3 Simulation and Measurement Results..... 98

4.3.1 A 5.8 GHz DRA Array..... 98

4.3.1.1 Input Impedance Modeling and DR Dimensions..... 98

4.3.1.2 Stub Extension and DRs Placments..... 101

4.3.1.3 Return Loss and Impedance Matching..... 103

4.3.1.4 Radiation Patterns..... 105

4.3.1.5 Gain..... 107

4.3.1.6 Summary of 5.8 GHz DRA Array 108
4.3.2 A 5.2-5.8 GHz Wideband DRA Array 109
4.3.2.1 Input Impedance Modeling and DR Dimensions 109
4.3.2.2 Stub Extension and DRs Placments 112
4.3.2.3 Return Loss and Impedance Matching 114
4.3.2.4 Radiation Pattern 116
4.3.2.5 Gain. ……...118
4.3.2.6 Summary of 5.2-5.8 GHz Wideband DRA Array 119
4.3.3 A 8.5 GHz Circularly Polarized DRA Arrays 120
4.3.3.1 Input Impedance Modeling and DR Dimensions 120
4.3.3.2 Stub Extension and DRs Placments 123
4.3.3.3 Return Loss and Impedance Matching 125
4.3.3.4 Radiation Pattern 127
4.3.3.5 Gain…….. 130
4.3.3.6 Axial Ratio 130
4.3.3.7 Summary of 8.5 GHz Circularly Polarized DRA Arrays 132
4.3.4 A 7-8 GHz Wideband Circularly Polarized DRA Array 133
4.3.4.1 Input Impedance Modeling and DR Dimensions 133
4.3.4.2 Stub Extension and DRs Placments 136
4.3.4.3 Return Loss and Impedance Matching 138
4.3.4.4 Radiation Pattern 140
4.3.4.5 Gain. ……..143
4.3.4.6 Axial Ratio 143

4.3.4.7 Summary of 7-8 GHz Wideband Circularly Polarized DRA Array 145

4.4 Summary 146

CHAPTER FIVE

CONCLUSIONS AND RECOMMENDATIONS 147

5.1 Conclusion 147

5.2 Research Contribution..... 148

5.2.1 Novelty of Gain Improvement and Reducing Size 148

5.2.2 Novelty of Wideband Operation 148

5.2.3 Novelty of Circular Polarization Radiation..... 148

5.2.4 Contribution of DRA Array Model..... 148

5.3 Recommendations..... 149

REFERENCES..... 150

LIST OF PUBLICATIONS……...168

APPENDICES Appendix A: Substrate datasheet

Appendix B: Antenna datasheet

Appendix C: Matlab input impedence calculations

Appendix D: S-parameter and input impedence measurements

Appendix E: Data tables of radiation pattern measurment

Appendix F: Data tables of Gain measurments

Appendix G: Data tables of axial ratio plot

LIST OF TABLES

		Page
Table 2.1	Comparison of circular polarized DRA arrays reported in the literature	48
Table 2.2	Comparison of wideband DRA arrays reported in the literature	55
Table 3.1	Compositions to produce of about 30 gm of CCTO	77
Table 3.2	Compositions to produce about 150 gm of ZST	78
Table 4.1	Calculated dielectric constant	97
Table 4.2	Comparison Result for Measured and Simulated of 5.8 GHz DRA Array	108
Table 4.3	Comparison Result for Measured and Simulated of 5.2-5.8 GHz Wideband DRA Array	119
Table 4.4	Comparison Result for Measured and Simulated of 8.5 GHz Circularly Polarized DRA Arrays	132
Table 4.5	Comparison Result for Measured and Simulated of 7-8 GHz wideband circularly polarized DRA Array	145

LIST OF FIGURES

Page

Figure 2.1	Typical dielectric resonator antennas and feeding mechanisms (Luk and Leung, 2002)	12
Figure 2.2	Coordinate convention and internal E and H field distribution. (a) Coordanate system convention. (b) Field distribution view at *xz* plane (c) Field distribution view at *xy* plane	16
Figure 2.3	(a) Dielectric guide (b) Cross sectional Field distribution (Marcatili, 1969)	18
Figure 2.4	Normalized resonant frequency of rectangular DRA (Petosa, 2007)	20
Figure 2.5	The radiation model of rectangular DRA (Luk and Leung, 2002)	22
Figure 2.6	Microstrip slot coupled rectangular dielectric resonator antenna (Ittipiboon et al., 1993)	24
Figure 2.7	Effect of substrate thickness and dielectric constant on the impedance bandwidth {VSWR⟨2} and radiation efficiency (Pozar, 1992)	26
Figure 2.8	Variation of radiation Q for a rectangular patch antenna as a function of substrate dielectric constant ,h=1.59 mm, W=0.9L, f=3 GHz. (Garg, 2001)	27
Figure 2.9	Variation of radiation Q for a rectangular patch antenna as a function of substrate thickness, ε_r=2.2 mm, W=0.9L, f=3 GHz (Garg, 2001)	27
Figure 2.10	A microstrip line coupled with rectangular slot (Sullivan & Schaubert, 1986)	30
Figure 2.11	Microstrip line geometry	31
Figure 2.12	Input impedance, current and voltage variation along short circuited microstrip line λ (Ganesan & Mole, 2010)	31
Figure 2.13	Linear array of DRAs fed by microstrip line (Petosa et al., 1998)	33
Figure 2.14	Aperture coupled DRA array (Keller et al., 1998)	33

Figure 2.15	Aperture-coupled cylindrical DR antenna: (a) Top view of E-plane array configuration (b) Top view of H-plane array configuration and (c) Side view of single element (Chow et al., 1995)	34
Figure 2.16	Four-element linear microstrip-coupled CDRA arrays. (a). Top view of configuration *A* shaping *E* at $\Theta=90^{o}$. (b) Top view u of configuration *B* shaping *E* at $\Phi=90^{o}$. (c) Side view of a microstrip-coupled single CDRA (Drossos et al., 1998)	35
Figure 2.17	Top and side view of Multi-layer branch line linear array of MSDRAs (Petosa et al., 1997)	37
Figure 2.18	Linear Array of Dielectric Resonator Elements Fed by Coaxial Probes (Junker et al., 1995)	38
Figure 2.19	Two-element broadside array using cylindrical DRA (a) E-plane Configuration (b) H-plane Configuration (Drossos et al., 1996)	38
Figure 2.20	Four element linear probe-fed CDRA (a) E-plane Configuration (b) H-plane Configuration (Drossos et al., 1998b)	39
Figure 2.21	Two elements array (a) E-plane Configuration (b) H-plane Configuration (Wu et al., 2001)	39
Figure 2.22	K-band prototype antenna (Birand & Gelsthorpe, 1981)	40
Figure 2.23	Dielectric image guide fed 20 elements array (Petosa et al., 1995a)	41
Figure 2.24	Geometry of the 15 DRA fed by DIG. (Al-Zoubi et al., 2010)	41
Figure 2.25	DRA pair-unit and its subarray (Haneishi and Takazawa, 1985)	42
Figure 2.26	Array of XDRA fed by sequential rotation (Petosa et al., 1996a)	43
Figure 2.27	Basic arrangement of array subunits (a) normal arrangement (b) subarray composed of paired units (Haneishi and Bing, 1999)	44
Figure 2.28	Geometry of the CP configurations (a) single CP element (b) 2X2-element subarray (Pang et al., 2000)	44
Figure 2.29	Different arrangement and feeding (a)-(e) of four element array of dielectric resonator, (f) sequential rotation (Kishk, 2003c)	45

Figure 2.30	The geometry of the elliptical DRA fed by DIG: (a) side view, (b) top view of single antenna, (c) top view of antenna array (Mousavi Kejani & Neshati, 2010)	46
Figure 2.31	Schematic illustrating a ground DR aperture coupled to a notched CPW fed: (a) single, (b) array (Lee & Simons 1993)	49
Figure 2.32	Linear array of DRAs fed by microstrip line (Petosa et al., 1996b)	50
Figure 2.33	Geometry of the construction the hexagon shaped upper resonator and triangle shaped lower resonator (Zhang et al., 2009)	51
Figure 3.1	Research methodology flowchart.	59
Figure 3.2	Voltage allocation over a microstrip line	60
Figure 3.3	Proposed three elements array principal showing the spacing between the elements (a) dielectric elements located on the coupling slots were omitted. (b) Dielectric elements located on the coupling slots	61
Figure 3.4	Geometry of the Single notched rectangular DRA (a) top view and (b) side view. (Ittipiboon et al., 1996) (c) Proposed notched wideband array	63
Figure 3.5	(a) Antenna geometry of aperture fed CP rectangular DRA element.(Oliver et al., 1995) (b) Proposed circularly polarized array.	65
Figure 3.6	Theoretical S_{11} return loss showing dual linear resonance (Oliver et al., 1995)	66
Figure 3.7	Geometry of the notched rectangular DRA with 45^{o} rotated slot coupled (a) top view and (b) side view. (Sheng-Ming and Ching-Long, 2005). (c) Proposed notched wideband circularly polarized array	67
Figure 3.8	Input impedance for different wavelengths of short circuited line (Ganesan and Sreeja Mole, 2010)	69
Figure 3.9	Discrete component resonator. (Kajfez and Guillon, 1986)	73
Figure 3.10	Equivalent circuit coupled to microstrip line (Collin, 1992)	74

Figure 3.11	(a) Equivalent circuit of microstrip slot coupled single DRA. (b) Equivalent circuit of microstrip slot coupled 3 element DRA array	75
Figure 3.12	Calcination profile for CCTO and ZST powders	79
Figure 3.13	Sintering profile for CCTO and ZST	80
Figure 3.14	The modeling of DRA array in ADS	83
Figure 3.15	Equipment setup for Return loss and impedance matching measurement	86
Figure 3.16	Equipment setup for radiation pattern measurement	88
Figure 4.1	XRD pattern of CCTO powder calcined at 900˚C for 720 minutes.	93
Figure 4.2	XRD pattern of ZST calcined at 700˚C for 720 minutes.	94
Figure 4.3	FESEM image of fracture surface of CCTO sample sintered at 900˚C for 720 minutes.	95
Figure 4.4	FESEM image of fracture surface of ZST sample sintered at 1300˚C for 360 minutes.	96
Figure 4.5	The 5.8 GHz DRA array model in ADS	100
Figure 4.6	The proposed 5.8 GHz DRA array structure. (a) Slots dimensions. (b) Microstrip dimensions (width=1.899), (c) and (d) Dielectric elements dimensions [all dimensions in mm]	101
Figure 4.7	The designed 5.8 GHz DRA array structure in CST (a) font view (b) back view (c) fabricated	102
Figure 4.8	The maximum power radiated antinodes over the microstrip at 5.8 GHz of the 5.8 GHz DRA array	103
Figure 4.9	Return loss for ADS Modeling, CST Simulation and Measurement of the 5.8 GHz DRA Array	104
Figure 4.10	The input impedance of the 5.8 GHz DRA array (a) simulated (b) measured	105
Figure 4.11	The E and H radiation patterns of the 5.8 GHz DRA array (a) simulated and (b) measured	106

Figure 4.12	The measured CST and simulated gain in dBi of the 5.8 GHz DRA.	107
Figure 4.13	The 5.2-5.8 GHz DRA array model in ADS	111
Figure 4.14	The proposed 5.2-5.8 GHz DRA array structure (a) Slots dimensions (width of the slots=1 mm). (b) Microstrip dimensions (width=1.86 mm), (c) and (d) Dielectric elements dimensions [All dimensions in mm]	112
Figure 4.15	The designed 5.2-5.8 GHz DRA array structure in CST (a) font view and (b) back view (c) fabricated	113
Figure 4.16	The maximum power radiated antinodes over the microstrip at 5.8 GHz of the 5.2-5.8 GHz DRA array.	114
Figure 4.17	Return loss for ADS Modeling, CST Simulation and Measurement of the 2.5-5.8 GHz wideband circularly polarized DRA Array	115
Figure 4.18	The input impedance of the 5.2-5.8 GHz DRA array (a) simulated (b) measured	116
Figure 4.19	The E and H radiation patterns of the 5.2-5.8 GHz DRA array (a) simulated (b) measured	117
Figure 4.20	The simulated and measured gain in dBi of the 5.2-5.8 GHz DRA.	118
Figure 4.21	The 8.5 GHz DRA array model in ADS.	122
Figure 4.22	The proposed 8.5 GHz DRA array structure in (a) Slots dimensions (width of the slots=1 mm) (dielectric omitted. (b) Microstrip dimensions (width=1.7 mm), (c) dielectrics lengths and widths (slots omitted) and (d) Dielectric elements heights. [All dimensions in mm].	123
Figure 4.23	The designed 8.5 GHz DRA array structure in CST (a) font view (b) back view (c) fabricated	124
Figure 4.24	The maximum power radiated antinodes over the microstrip at 8.5 GHz of the 8.5 GHz DRA array.	125
Figure 4.25	Return loss for ADS Modeling, CST Simulation and Measurement of the 8.5 GHz circularly polarized DRA Array	126
Figure 4.26	The input impedance of the 8.5 GHz DRA array (a) Simulated (b) measured	127

Figure 4.27	The simulated (a) E-co and E-Cross radiation patterns (b) H-co and H-Cross radiation patterns of the 8.5 GHz DRA array	129
Figure 4.28	The measured (a) E-co and E-Cross radiation patterns. (b) H-co and H-Cross radiation patterns of the 8.5 GHz DRA array	129
Figure 4.29	The measured and simulated gain in dBi of DRA of the 8.5 GHz DRA array	130
Figure 4.30	Simulated and measured axial ratio 8.5 GHz DRA array	132
Figure 4.31	The 7-8 GHz wideband circularly polarized DRA Array model in ADS	135
Figure 4.32	The designed structure of the 7-8 GHz wideband circularly polarized DRA Array (a) Slots dimensions (width of the slots=1 mm). (b) Microstrip dimensions (width=1.7 mm), (c) and (d) Dielectric elements dimensions. [All dimensions in mm]	136
Figure 4.33	The designed 7-8 GHz wideband circularly polarized DRA Array in CST (a) front view (b) back view (c) fabricated	137
Figure 4.34	The maximum power radiated antinodes over the microstrip at 7.5 GHz of the 7-8 GHz wideband circularly polarized DRA Array	138
Figure 4.35	Return loss for ADS Modeling, CST Simulation and Measurement of the 7-8 GHz wideband circularly polarized DRA Array	139
Figure 4.36	The input impedance of the 7-8 GHz wideband circularly polarized DRA Array (a) simulated (b) measured	140
Figure 4.37	The simulated radiation patterns of the 7-8 GHz wideband circularly polarized DRA Array. (a) E-co and E-Cross radiation patterns at 7.5 GHz. (b) H-co and H-Cross radiation patterns at 7.5 GHz	142
Figure 4.38	The measured radiation patterns of the 7-8 GHz wideband circularly polarized DRA Array (a) E-co and E-Cross radiation patterns at 7.5 GHz. (b) H-co and H-Cross radiation patterns at 7.5 GHz	142
Figure 4.39	The simulated and measured gain in dBi of the 7-8 GHz wideband circularly polarized DRA Array	143
Figure 4.40	Simulated and measured axial ratio of the 7-8 GHz wideband circularly polarized DRA Array	144

LIST OF SYMBOLS

ε_r	Dielectric constant
ε_{eff}	Effective dielectric constant
Ω	Ohms (Impedance)
β	Propagation constant
λ_0	The wavelength in free space
λ_g	The guided wave length
Γ	Reflection coefficient
η	The radiation efficiency
ω	Resonance frequency
B_m	The susceptance of the fringing field capacitance of the microstrip
C	Light speed
C_l	Capacitance of the microstrip
C_r	capacitance of dielectric resonator
E	Electrical field
E_θ	Vertical radiation plane
E_ϕ	Horizontal radiation plane
E_{SC}	Electrical at short circuit
f_o	Resonant frequency
G_{rm}	Microstrip radiation conductance

G_S	Gain of standard antenna
G_T	Gain of tested antenna
H	Magnetic field
K	The effective propagation constant of the line
k_o	The free-space wave number
$k_{x,}$	Wave number in X direction
k_y	Wave number in Y direction
k_z	Wave number in Z direction
L_r	Inductance of dielectric resonator
M	Mutual coupling
P_m	The magnetic dipole moment of the DRA
P_{rad}	Radiated power of rectangular DRA
P_S	Power received by the standard antenna
P_T	Power received by tested antenna
Q	Quality factor
R_r	Resistive of dielectric resonator
S	Stub extension
S_1	Stub extension which to half wave length
S_2	Stub extension equals to quarter wave length
S_x	Elements spacing in the X direction

S_y	Elements spacing in the Y direction
W_e	Stored energy in dielectric resonator
X_S	Stub length
Z_0	The microstrip input impedance
Z_{SC}	Impedance at short circuit end
Z_{slot}	Impedance of slot

LIST OF ABBREVIATIONS

ADS	Advanced design system
AF	Array factor
AR	Axial ratio
BW	Bandwidth
CCTO	$CaCu_3Ti_4O_{12}$
CP	Circular polarization
CST	Computer simulation technology
DIG	Image guide feed
DR	Dielectric resonator antenna
DRA	Dielectric resonator antenna
MSDRA	Multi-Segment Dielectric resonator antenna
MPA	Microstrip patch antenna
LHCP	Left-hand circular polarization
LP	Linearly polarized
RHCP	Right hand circular polarization
FESEM	Field Emission Scanning Electron Microscopy
SLL	Side lobe level
SWR	Standing wave ratio
TE	Transverse electric
TM	Transverse magnetic
VSWR	Voltage standing wave ratio
WLAN	Wireless local area network

XDRA	Cross dielectric resonator antenna
XRD	X-ray diffraction
ZST	$Zr_{0.6}Sn_{0.4}TiO_4$

REKABENTUK DAN PEMODELAN TATASUSUNAN ANTENA PENYALUN DIELEKTRIK MENGGUNAKAN KAEDAH BARU PENYUAP MELALUI SEBUAH MIKROSTRIP TAMAT PINTAS

ABSTRAK

Antena Penyalun Dielektrik (APD) telah dibangunkan bagi kegunaan didalam jalur frekuensi gelombang mikro dan milimiter kerana ciri-ciri radiasi yang menarik. Walau bagaimanapun, biasanya APD adalah antena gandaan rendah, kerana itu APD boleh ditatasusunkan bagi mencapai gandaan yang lebih tinggi. Manakala kebanyakan teknik tatasusunan APD telah menunjukkan kejayaan yang terhad untuk mengurangkan saiz tatasusunan dan kerumitan rekaan. Kajian ini memberi tumpuan kepada pembangunan dan pemodelan APD dari tatasusunan novel penyalun dielektrik (PD) untuk meningkatkan gandaan antena dan mengurangkan saiz tatasusunan. Susunan mudah ini juga boleh digunakan untuk mencapai salunan jalur lebar dan polarisasi berkeliling yang selari dengan penambahbaikan gandaan. Tatasusunan APD telah di uja oleh garis mikrostrip dengan beberapa slot berganding diletakkan di atas satah bumi logam. Untuk meningkatkan gandaan, kedudukan slot telah ditentukan berdasarkan ciri-ciri peruntukan voltan melalui penyuap mikrostrip tamat pintas. Empat rekabentuk tatasusunan telah dibangunkan dalam kajian ini. Kaedah penyuapan yang baru ini boleh dipakai untuk meningkatkan lebar jalur atau memperolehi polarisasi berkeliling. Penyalun dielektrik telah digunakan untuk meningkatkan lebar jalur manakala unsur-unsur dielektrik telah diputarkan 45^{o} dengan merujuk kepada sisi-sisi slot yang di ujakan untuk menjana corak polarisasi berkeliling. Struktur tatasusunan APD telah dimodelkan kedalam litar selari salunan RLC dengan menggunakan perisian Agilent ADS. Pemodelan telah digunakan untuk mengira dimensi PD. Ciri-ciri tatasusunan APD

daripada simulasi menggunakan CST Microwave Studio dan pengukuran termasuk kehilangan pulangan, corak radiasi dan gandaan antena telah dibentangkan. Rekabentuk APD tatasusunan 5.8 GHz menghasilkan gandaan 8.8 dBi dengan saiz struktur 60x40 mm. Rekabentuk APD tatasusunan lebar jalur 5.2-5.8 GHz menghasilkan gandaan maksima 8.29 dBi didalam lebar jalur galangan jalur lebar sebanyak 27 % dengan saiz struktur 60x40 mm. Rekabentuk APD tatasusunan polarisasi berkeliling 8.5 GHz menghasilkan gandaan 8.5 dBi dengan lebar jalur nisbah paksi sebanyak 2.9 % dan saiz struktur 40x50 mm. Rekabentuk APD tatasusunan polarisasi berkeliling lebar jalur 7-8 GHz menghasilkan gandaan maksima 9.45 dBi dalam lebar jalur galangan jalur lebar sebanyak 12.1 %. Sebagai tambahan, lebar jalur nisbah paksi adalah sebanyak 13.6% dengan saiz struktur 40x40 mm. Persetujuan yang baik telah diperhatikan di antara keputusan simulasi dan pengukuran. Rekabentuk-rekabentuk tersebut adalah mudah untuk difabrikasikan jika dibandingkan dengan rekabentuk-rekabentuk APD yang terdahulu disebabkan penggunaan teknik penyuapan yang baru. Pengurangan saiz juga adalah signifikan jika dibandingkan dengan rekabentuk-rekabentuk yang telah dilaporkan didalam kajian ilmiah.

DESIGN AND MODELING OF DIELECTRIC RESONATOR ANTENNA ARRAY USING NEW FEEDING METHOD OVER A SHORT ENDED MICROSTRIP

ABSTRACT

Dielectric resonator antennas (DRAs) were developed for the use in the microwave and millimeter frequency band due to their attractive radiation characteristics. However, DRA are typically low gain antennas therefore DRA can be arrayed to achieve higher gain. Whereas, most of the DRA array techniques showed a limited success to reduce the array size and decrease the design complexity. This work focused on development and modeling of a dielectric resonator antenna (DRA) array from a novel arrangement of the dielectric resonators (DRs) to enhance the antenna gain and reducing array size. This simple arrangement also can be used to achieve wideband resonant and circular polarization in parallel with improved gain. The DRA array was excited by a microstrip line with few coupled slots positioned on the top of a metallic ground plane. To improve the gain, the slot positions were determined based on the characteristics of voltage allocation over a short ended microstrip feeder. Four array designs were developed in this work. This new feeding method can be employed to enhance the bandwidth or acquiring circular polarization. The Notched dielectric resonators were used to enhance the bandwidth while dielectric elements were rotated 45° with respect to the sides of the exciting slots to generate the circular polarization pattern. The DRA array structure was modeled into a parallel RLC resonant circuit using Agilent ADS software. Modeling is used to only calculate the dimensions of the DRs. Characteristics of the DRA arrays from simulation using CST microwave studio and

measurements including return loss, radiation patterns and antenna gain are presented. The 5.8 GHz DRA Array design possesses an 8.8 dBi gain with structure size of 60x40 mm. The 5.2-5.8 GHz Wideband DRA Array design possesses a maximum gain of 8.29 dBi within wideband impedance bandwidth of 27 % with structure size of 40 x 60 mm. The 8.5 GHz Circularly Polarized DRA Array design possesses a gain of 8.51 dBi with axial ratio bandwidths of 2.9 % and structure size of 40X50 mm. The 7-8 GHz wideband circularly polarized DRA Array design possesses a maximum gain of 9.45 dBi with a wideband impedance bandwidth of 13.59 %. In addition, the axial ratio bandwidth was 13.69 % with structure size of 40x40 mm. A good agreement was observed between the simulated and measured results. The designs were simple and easy to fabricate compared with the existing works on DRA arrays due to use of the new feeding technique. The size reduction was also significant when compared with previous works reported in the literature.

CHAPTER ONE

INTRODUCTION

1.1 Background

The present-day technology demands continuing growth in electronic systems operating in the RF and microwave spectrum. These systems are designed to provide high efficiency, wide bandwidth and reduced equipment size. Recent advances in wireless communications have resulted in development of antennas that can be embedded into wireless products. Since the last two decades, two classes of antennas i.e., the microstrip patch antenna (MPA) and the dielectric resonator antenna (DRA) have been under investigation for modern wireless applications. The MPA is popular since it provides lightweight and conformal antennas for millimeter-wave applications. However, there are some detrimental factors, these include; wide beamwidth, narrow bandwidth, surface wave excitation, and conductor losses. Attempts to reduce these negative effects have proven to achieve limited success, since an increase in one aspect usually comes with degradation in another factor. The largest detrimental effect at millimeter-wave frequencies continues to be conductor losses, thus reduced radiation efficiency.

In the early 1980's, Stuart Long developed the dielectric resonator antenna (DRA) (Long et al., 1983). The DRA is a resonant antenna, fabricated from a high-permittivity dielectric ceramic material mounted on a ground plane and fed by a coaxial probe (McAllister et al., 1983), slot coupling (Leung and To, 1997) or a microstrip line in the ground plane (Harith, 2005). Different geometries of the DRA such as

rectangular, cylindrical, hemispherical, circular, triangular and other shapes are possible. The resonant frequency of the DRA is a function of size, shape and material permittivity. Dielectric resonator antenna is an excellent radiator as it has negligible metallic loss. It offers advantages such as small size, wide bandwidth, low cost and compatibility with the existing feeding techniques when operated at millimeter wave frequencies.

Some applications require low profile, low cost and high gain. Since the gain of a single DRA antenna is limited to approximately 5 dBi (Luk & Leung, 2002), an array can be used to produce a higher gain. With appropriate feed arrangements, the DRA elements can be used to form DRA arrays with directional radiation patterns providing enhanced antenna gain and bandwidth for telecommunication applications. An array with efficient radiators and efficient fed network would satisfy the requirements.

1.2 Problem Statement

Current commercially available wireless local area network (WLAN) access points that use the dipole antenna, monopole antenna or MPA exhibit some physical and network limitations. The movable dipole or monopole antenna itself has clear physical structure limitation. The moving and tilting of the antenna pole changes the radiation pattern that requires frequent recalibration which will make maintenance support difficult. On top of that, it is susceptible to physical damage as the antenna pole is easily bent or broken. The monopole antenna generates an omnidirectional radiation pattern characteristic which can penetrate the wall. This may reduce the efficiency as the

propagation envelope for a specific room or area is reduced. Both the physical limitation and the propagation envelope reduction will reduce the reliability of equipment and the wireless network. For that, the DRA become as a good candidate for wireless applications since it can overcome current limitations of wires antennas and MPA.

Normally, single pellet DRA has a low gain (5 dBi) and narrow bandwidth (Luk & Leung, 2002). In the other hand, wireless applications systems require higher antenna gain, wider bandwidth and circular polarization in some applications. Thus, DRA arrays have to resolve three major objectives namely: high gain, wideband operation and circular polarization. The design complexity, size reduction and low price are major goals taken into consideration.

The DRA array designs documented in the literature showed a limited success to reduce the array size and feeding network complexity. Therefore, a new feeding method is required to overcome these limitations. The new feeding technique favored to be applicable for any of the major goals covered by the DRA array. Likewise, the new feeding technique have to contribute for the design simplicity as well as the size reduction.

1.3 Objectives

The aim of this research is to design a DRA array in the bands IEEE 802.11a band (5.180-5.805 GHz) and IEEE 802.15.4 (Europe) **(**6-8.5 GHz), with gain

improvement and some reduction of the antenna size by using the voltage allocation over short ended microstrip feeding rectangular dielectric resonators (DRs). Table 1.1 summarize the selected frequency band and related applications. In parallel, new method for calculating the rectangular DR dimensions is introduced by assuming an approximate input impedance model for rectangular DR feed by microstrip slot coupled. The achievement of the main goal will include the accomplishment of the objectives listed down as below:

a) To design an enhanced gain DRA array using the new feeding method. This feeding method must be unique and contribute to the size reduction and simplicity of the designed DRA arrays.
b) To propose an equivalent model of DRA array to be used as a new method to calculate the dimensions of the DRs.
c) To design a unique wideband DRA arrays using the new feeding method.
d) To design a unique circularly polarized DRA arrays using the new feeding method.

1.4 Research Scope and Limitations

The scope of this project focused on the design of the microstrip slot coupled fed DRA array. All the designs are excited with serial microstrip slot coupled because this feeding mechanism is the simplest among other feeders. The feeding network is etched on two different substrates, Duroid RO4003C® with relative permittivity (ε_r=3.38) and FR4 with relative permittivity of (ε_r=4.55).

A profound study of the on the current research and depth of the literature review of DRA array and there applications. A number of methods used for designing DRA array for various applications in microwave wireless communications. A thorough study for different feeding techniques used to couple the DRs for obtaining a strong coupling between the DRs and the feed network.

In the first stage of the project, a review on the dielectric material and DRA was performed to smooth the progress of fabrication. The DRs used in this project are fabricated from two different materials. These dielectric materials are known as zirconium tin titanate (ZST) and calcium copper titanate (CCTO).

The second stage was the modeling of the DRA array microstrip slot coupled. This model was established by calculating the array sub elements, DR, microstrip and slot, impedances. A thorough review on the equations representing the array sublements relative impedances. Later on, Agilent ADS to represent the model while Matlab® was used to calculated the DRs dimensions.

The third stage was the simulation using CST microwave studio. This includes building the DRA array based on related parameters, dimensions and permittivity's, to represent the design behavior as a radiator. CST software allows the designer to obtain the return loss, radiation pattern and gain characteristics of the designed antenna before its fabricated.

The last stage was the measurements of the antenna characteristics. The setup of the return loss, radiation pattern and gain measurement have to be well understood. The results from measurement is compared with those from simulation and conclusion was made.

The limitations were represented in choosing the substrate based on thickness and permittivity, as well in the dielectric materials based the on dielectric constant. In the measurements, limitations represented in finding a standard known gain antennas.

1.5 Thesis Contribution

The main contribution of this research would be the design of a novel antenna feeding technique with an improved gain as well as size reduction capability. The DRA array structure and design should be simple and realizable. Therefore, the contributions of this thesis are as follows:

a) Modeling of DRA array in Agilent Advanced Design System with configurability of different resonant frequencies, which helps to understand and predict the operating frequency
b) The development of wideband enhanced gain DRA arrays with size reduction of the antenna structure, which makes antenna fit for WIFI applications in wireless systems.

c) The development of circularly polarized enhanced gain DRA arrays as well as small size of antenna which can be used for certain applications that require movable antennas such as radar systems.

1.6 Thesis Outline

The report has been divided into a total of five chapters. Chapter one begins with brief introduction of the recent trend in antenna technology and dielectric antenna in the wireless communication. This chapter also has laid out the background as to why this research was carried out and outlined the expected goals of the study.

The thesis is organized as follows:

Chapter Two provides a theoretical background and detailed literature review. The theoretical background includes the theory of DRA and its features, detailed explanations of the array sub-elements as rectangular DR, slot and substrate effect. The literature review shows the previous studies on DRA arrays and ensures that the designs of this project will not repeat these existing works. Since the wideband and circular polarization are other complimentary objectives of this research, a detailed related literature also been reported.

Chapter Three provides a detailed explanation on the proposed DRA input impedance model and array structures. The experimental methodology, which includes the fabrication process to produce ceramic DRs from different material composition,

simulation procedure which was done using ADS and CST software and measurement setup are explained.

Chapter Four discusses in details result of proposed DRA arrays from both the simulation and measurement. Various measurements for DR fabricated from different materials are also displayed and discussed. The simulation results in term of return loss, radiation pattern and gain have been generated. Comparison are made between measurement and simulation result.

Chapter Five summarizes the result of the designs in terms of gain, bandwidth, and polarization of the DRA arrays. The intent therefore, is to analyze whether the aims of the project are achieved or not. Finally, notable suggestions for further works are recommended.

CHAPTER TWO

LITERATURE REVIEW

2.1 Introduction

In 1939, R.D Richtmyer showed that un-metalized dielectric bodies could execute like the metallic cavities, which he called dielectric resonators. If excited at specific frequencies, the dielectric resonators can be made to radiates very impressively (Long et al., 1983). For the dielectric resonator antenna, the radiating mechanism is a displacement current circulating in a dielectric medium. The energy stored in the dielectric material is very high, and it is difficult for external objects to disturb the resonance of the material.

The usage of dielectric resonators as antennas has benefits such as minimal ohmic losses, smaller size than conventional antennas by the influence of the square root of the dielectric constant of the material (ε_r), high radiation effectiveness and improved bandwidth. For dielectric constants, $10< \varepsilon_r <100$, the antenna size can be around 5-10 times smaller than the conventional antennas. The losses for a DRA are the dielectric loss due to imperfect dielectric material which is a negligible and ohmic loss occurring in the feed mechanisms and the ground plane currents. Due to their well-matched resonances, the DRAs are characterized by excellent return losses. The impedance bandwidth for a DRA is a function of the material's permittivity and aspect ratio (length-to-height ratio) (Petosa et al., 1998). Furthermore, for a given material permittivity ε_r adjusted to provide compact low profile providing and or a wideband

antenna. Size is reduced with higher permittivities and bandwidth is increased using low permittivities.

As compared to the microstrip antenna, the DRA has a wider impedance bandwidth. For a simple rectangular DRA, a bandwidth of 10% can be achieved for a dielectric constant of 10 or less (Petosa et al., 1998). The microstrip antenna radiates through two narrow edges of the patch whereas the DRA radiates through its entire surface except the grounded part. Surface waves are absent in the DRA as compared to the microstrip antenna (Richtmyer, 1939) resulting in better efficiency and fewer distortions in the radiation pattern. However, many common characteristics exist between the microstrip antenna and the DRA because both have resonant cavities. By increasing the permittivity , ε_r , both of them can be made small, since the dielectric wavelength is smaller than the free space wavelength by a factor of $1/\sqrt{\varepsilon_r}$. However by using high permittivity material for the microstrip antenna, the bandwidth becomes extremely narrow. The excitation mechanisms employed for the microstrip antenna are compatible with the DRAs (Richtmyer, 1939).

2.1.1 Dielectric Resonator Antenna

The dielectric resonator antenna (DRA) is simply a block of low-loss dielectric placed on a ground plane. A precursor was probably a short monopole surrounded by a centered cylindrical dielectric; the monopole is the same height as the Dielectric (James & Burrows, 1973). As expected, a short monopole may be resonated by high ε, but the

bandwidth is reduced. (Long et al., 1983) introduced the DRA, where the dielectric body is resonant.

The DRA can be formed in different shapes and coupled with many methods. A rectangular block DRA can be fed by a probe (Kakade & Ghosh 2011) or fed by a microstrip (Fwen Hoon et al 2012) (Mridula et al., 2004a), or by a microstrip line with a tee (Bijumon et al., 2005). Circular disk DRA (McAllister et al., 1983) have been fed by a microstrip excited slot (Baba et al, 2013 , Leung & To, 1997); an inverted microstrip (Leung et al., 1997); a waveguide with a slot in the guide top wall-ground plane (Eshrah et al., 2005b); a waveguide with a probe extending into both the guide and the DRA (Eshrah et al., 2005a) ; and a vertical metal strip on the disk exterior, with the strip connected to a feed line (Ng and Leung, 2002). Also other DRA shapes include a hemisphere fed by a slot in the ground plane with microstrip excitation (Kwok-Wa et al., 1995); a half-cylinder with axis parallel to the ground plane and fed by a probe (Ruan et al., 2007, Mongia, 1989) ; a cylindrical ring with axis normal to the ground plane and fed by a microstrip (Leung et al., 1997); and conical dielectric shapes. Figure 2.1 shows different shapes of DRs and different coupling methods.

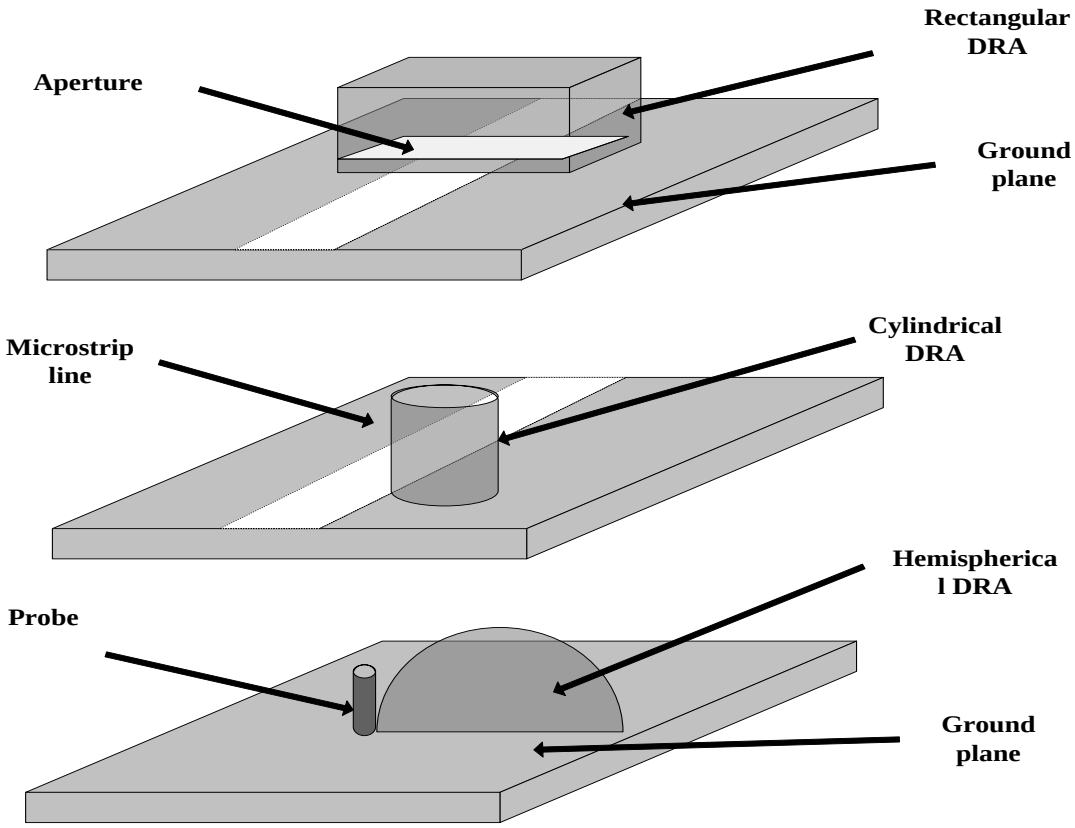

Figure 2.1: Typical dielectric resonator antennas and feeding mechanisms (Luk & Leung, 2002)

2.1.2 Features

Dielectric resonator antenna has many appealing features, which make it as one of the alternative antenna technologies in the wireless communication field (Petosa et al., 1998). Some of the attractive features are listed below (Cuhaci et al., 1996, Kishk, 2003a, Petosa, 2007, Petosa et al., 1998).

a) The volume of the DRA is proportionate to the dielectric constant of the material which can be varied from about 8 to 100 allowing more control over the

size and bandwidth of DRA. DRA size reduces when the dielectric constant increase.

b) DRA suffers from nearly no dissipation losses and there is no surface wave losses, which lead to high radiation productivity and wide bandwidth.
c) Various excitation mechanisms can be used (probes, slots, microstrip lines) to excite DRA which make it easy to integrate with many existing technologies.
d) Various shape of dielectric resonator can be designed (triangular, hemispherical, etc.) offering more degrees of freedom to the design.
e) Various modes can be excited leading to the different radiation characteristics. These modes can be controlled by using different excitation mechanisms.

2.1.3 Rectangular DRA

The rectangular DRA is the most versatile since it has two degrees of freedom. For any given resonant frequency and fixed dielectric constant, two of the three dimensions of the rectangular DRA can be chosen independently.

2.1.3.1 Field Modes

All resonators have a series of resonant modes or field structures, which are determined by their electrical characteristics and the boundary conditions. Van Bladel (Van Bladel, 1975a, Van Bladel, 1975b) investigated DRAs of arbitrary shapes with very high permittivity's, and concluded that there were two field modes in which the DRA could be classified. These are the confined and non-confined modes. The classification criteria at interface boundaries the following conditions are met;

- $\bar{E}.\hat{n} = 0$ and
- $\hat{n} \times \bar{H} = 0$

Condition a., where E denotes the electric field intensity and n denotes the normal to the surface of the resonator, is satisfied for both confined and non-confined modes. This condition states that there is no electric field intensity normal to the boundary. Condition b., where H denotes the magnetic field intensity, is only satisfied for confined modes. This condition indicates that the magnetic field is normal to the boundary. Van Baldel further states that the lowest order non-confined and confined modes act like magnetic and electric dipoles respectively. Finally, Van Baldel showed that confined modes can only be supported by dielectric elements exhibiting axial-symmetric properties. These modes or field structures are often classified as H and E modes. The H modes, corresponding to the non-confined case above, have a large magnetic field perpendicular to the interface, with the lowest order mode resembling a magnetic dipole in field structure. The E modes, confined, do not have this large magnetic field and the lowest order mode resembles an electric dipole.

Okaya and Barash (1963) first classified the H mode to belong to the transverse magnetic (TM) family and the E modes to the transverse electric (TE) family , however, later work by Hung Yuet (1965) used the opposite notation. This second convention continues to be used today, with two or three subscripts to identify the specific mode order. The subscripts denote the field variations in the appropriate orthogonal component, depending on the coordinates system used, spherical, cylindrical or rectangular. Cylindrical and spherical DRAs support both TE and TM modes, which,

when combined together form an additional hybrid family of modes. These degenerate modes in which two modes exhibit the same resonant frequency and thus interact with each other, result in a lack of mode purity. Various configurations of dielectric materials have been investigated (Mongia & Bhartia, 1994), with the theoretical emphasis placed on cylindrical or hemispherical shapes. The reason for this is the ability to generate closed form analytical solutions for axial-symmetric shapes. Since the focus of this thesis is rectangular DRAs, the remainder of the discussion and analysis will deal solely with this geometric shape.

From Van Bladel's work, the rectangular DRA, since it is not axial-symmetric, can only support non-confined (TE or H) modes and the radiation pattern of the lowest order mode should resemble that produced by a magnetic dipole. Also, since the rectangular shape cannot be defined as a body of revolution, a closed form solution is impossible. Thus, approximation methods are required to analyze the rectangular DRA. Considerable experimental work has been conducted on rectangular DRAS, which further emphasize these findings (St. Martin et al., 1990 , Mongia, 1992, Ittipiboon et al., 1993, Keller et al., 1995).

Although the rectangular DRA cannot be completely characterized analytically, they have an advantage over DRAs of other shapes. Since the rectangular DRA has three independent dimensions (two for cylindrical and one for spherical), the choice of these dimensions can be made to ensure that the resonant frequencies of the modes are separated apart from one another.

Thus, rectangular DRAs will not suffer from the mode degeneracy problem exhibited by other shapes. TE^X, TE^Y and TE^z modes are possible. Figure 2.2(a) provides the coordinate convention used in this thesis while Figure 2.2(b) and 2.2(c) show the directions associated with electric and magnetic fields expected of a rectangular DRA.

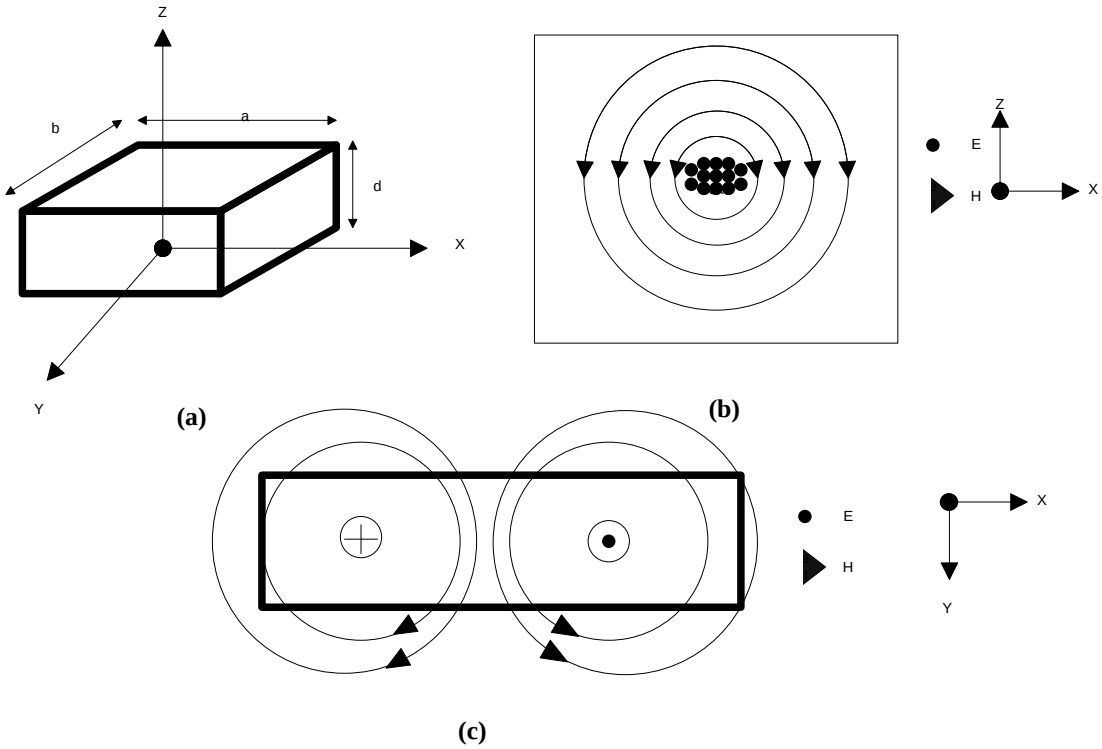

Figure 2.2: Coordinate convention and internal E and H field distribution. (a) Coordanate system convention. (b) Field distribution view at *xz* plane (c) Field distribution view at *xy* plane

For a rectangular DRA with dimensions *a*, *b* > *d*, the lowest order mode will be $TE^z_{11\delta}$. Using the dielectric waveguide model, this leads to the following fields within the DRA (Mongia & Ittipiboon, 1997):

$$H_x = \frac{(k_x k_z)}{j\omega\mu_0}\sin(k_x x)\cos(k_y y)\sin(k_z z) \tag{2.1}$$

$$H_y = \frac{(k_y k_z)}{j\omega\mu_0}\cos(k_x x)\sin(k_y y)\sin(k_z z) \tag{2.2}$$

$$H_z = \frac{(k_x^2 + k_y^2)}{j\omega\mu_0}.\cos(k_x.X)\cos(k_y.Y)\cos(k_z Z) \tag{2.3}$$

$$E_x = k_y \cos(k_x.X)\sin(k_y.Y)\cos(k_z Z) \tag{2.4}$$

$$E_y = -k_x \sin(k_x.X)\cos(k_y.Y)\cos(k_z Z) \tag{2.5}$$

$$E_z = 0 \tag{2.6}$$

$$\varepsilon_r k_o^2 = k_x^2 + k_y^2 + k_z^2 \tag{2.7}$$

$$k_z \tan\left(k_z.d/2\right) = \sqrt{(\varepsilon_r - 1)k_o^2 - k_z^2} \tag{2.8}$$

The $e^{j\omega t}$ time dependence is assumed in the above equations. The value δ can be defined as the fraction of a half cycle of the field variation in the z-direction and is given by:

$$\delta = \frac{k_z}{\pi/d} \tag{2.9}$$

2.1.3.2 Dielectric Waveguide Model for Rectangular DRAs

The dielectric waveguide model was first proposed by Marcatili (1969) to determine the guided wavelength in dielectric guides with rectangular cross-section. The dielectric guide is shown in Figure 2.3(a), having a rectangular cross-section of width *a* in the x-direction, height *b* in the y-direction and the waves propagating in the

z-direction. The field modes in the guide can be divided into TEy *mn* and TMy *mn*, (where *m* and *n* denotes the number of field in the x and y-direction, respectively inside the guide). The fields within the guide are assumed to vary sinusoidally, while the fields outside the guide are assumed to decay exponentially. To simplify the analysis, the fields in the shaded regions of Figure 2.3(b) are assumed to be zero.

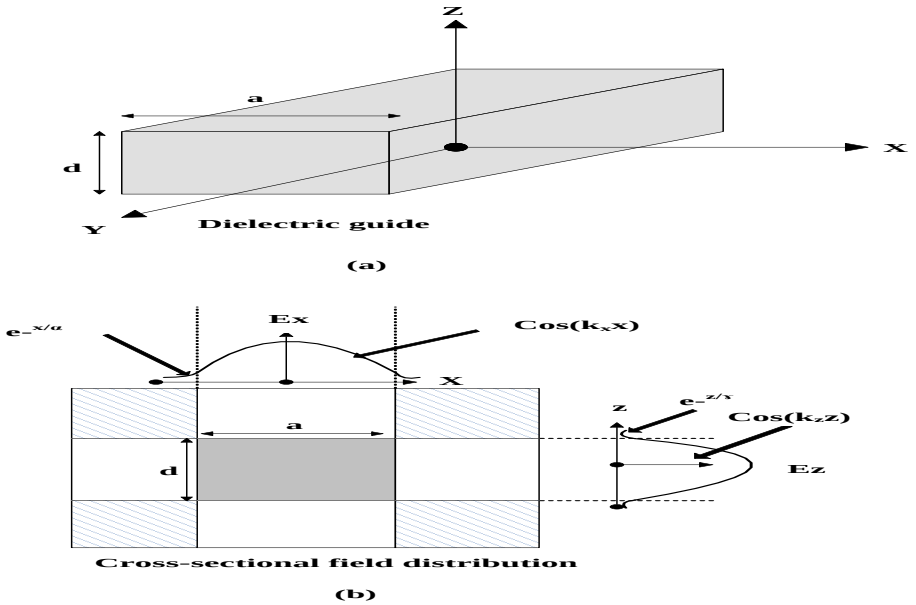

Figure 2.3: (a) Dielectric guide (b) Cross sectional Field distribution (Marcatili, 1969)

By matching the fields at the boundary conditions, the wave propagation numbers in the *x*-, *y*-, and *z*-directions ($k_{x,}k_y$, and k_z) (for $|x| \leq a/2$ and $|z \leq d/2$) and the attenuation constants in the *x*- and *z*-directions (α, γ) (for $|x| \geq a/2$ and $|z| \geq d/2$) can be determined, using Equation 2.7 as stated in (Marcatili, 1969):

where k_o is the free-space wave number given by:

$$k_o = \frac{2\pi}{\lambda_o} = \frac{2\pi f_o}{c} \tag{2.10}$$

Where c is the speed of light in free space, f_o is the operating frequency, and λ_o is free space wavelength. For well-guided modes, the fields are confined within the guide and a further approximation can be made:

$$k_x = \frac{m\pi}{a}, k_z = \frac{n\pi}{d} \tag{2.11}$$

This approximation is equivalent to assuming that magnetic walls exist at $x = \pm a/2$ and $z = \pm d/2$.

For a given resonant frequency f_o and resonator parameters E, a and d, the wave number k, can be determined. The dimension d can then be determined- Conversely, for a given resonator with parameters E, and dimensions a, b, and d, the resonant frequency can be determined in an iterative manner. These equations provide the basic analytical approximations, based on the model chosen, to characterize the electromagnetic properties of the rectangular DRA. Although not directly used in the remainder of this specific research, this analytical model is important to provide comparison values in which to validate the numerical simulation results. A more detailed and rigorous development of this model can be found in (Mongia, 1992) (Kumar Mongia and Ittipiboon, 1997).

2.1.3.3 Resonant Frequency

Equation 2.8 have been used to plot the curves in Figure 2.4. These curves plot the normalized frequency *F* versus the ratio of DRA dimensions *d/b* for various ratios of *a/b*. The normalized frequency is defined as (Petosa, 2007):

$$F = \frac{2\pi f_0 \sqrt{\varepsilon_r}}{c} \tag{2.12}$$

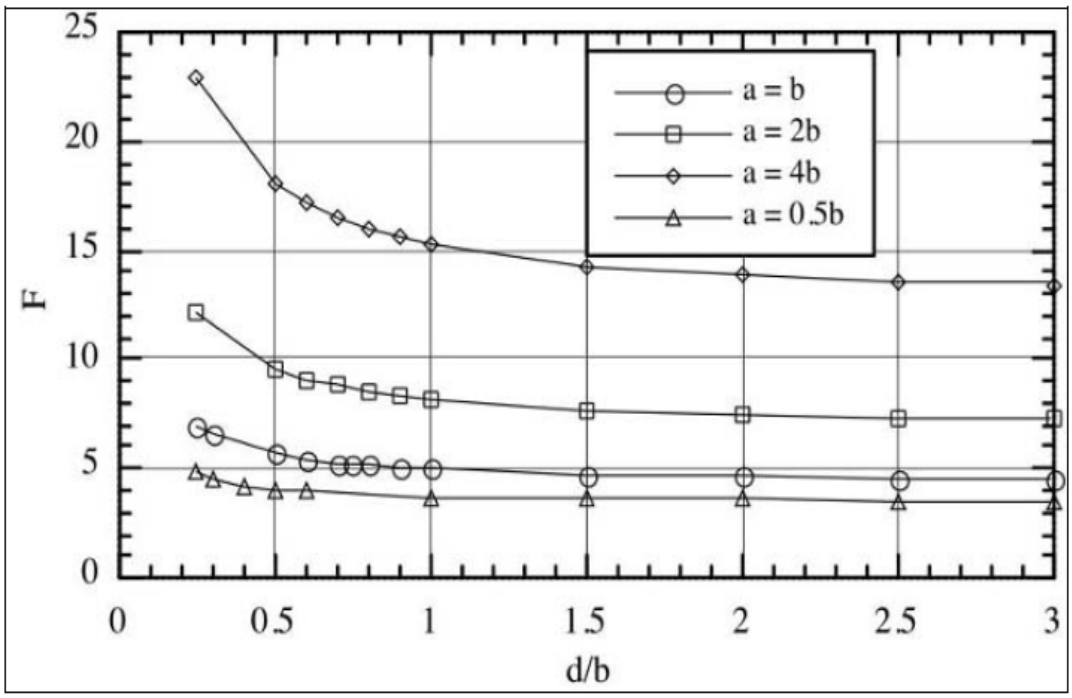

Figure 2.4: Normalized resonant frequency of rectangular DRA (Petosa, 2007)

2.1.3.4 Q-Factor

The radiation Q-factor of the rectangular DRA is determined using Mongia & Ittipiboon (1997)

$$Q = \frac{2\omega W_e}{P_{rad}} \tag{2.13}$$

where W_e and P_{rad} are the stored energy and radiated power, respectively and are expressed as:

$$W_e = \frac{\varepsilon_o \varepsilon_r abd}{32}\left(1+\frac{\sin(k_z d)}{k_z d}\right).\left(k_x^2 + k_y^2\right) \tag{2.14}$$

$$P_{rad} = 10k_o^4 \left|\rho_m\right|^2 \tag{2.15}$$

where:

ρ_m is the magnetic dipole moment of the DRA

abd are the DR length, width and height

$$\rho_m = \frac{-j\omega 8\varepsilon_o\left(\varepsilon_r - 1\right)}{k_x k_y k_z}.\sin(k_z d/2) \tag{2.16}$$

The impedance bandwidth (BW) of the DRA can be determined estimated from the radiation Q-factor using:

$$BW = \frac{VSWR - 1}{Q\sqrt{VSWR}} \tag{2.17}$$

where $VSWR$ is the maximum acceptable voltage standing-wave ratio

2.1.3.5 Radiation Model

The field distribution of the lowest order mode of the rectangular DRA, determined by the dielectric waveguide model equations, is similar to that of a short magnetic dipole. The radiation patterns generated by the DRA can therefore be approximated using the short magnetic dipole. Figure 2.5 depicts the equivalent model for a rectangular DRA mounted on an infinite ground plane. This corresponds to a

horizontal magnetic dipole aligned along the z-axis (Figure 2.5 (b)). The resulting radiation patterns (Figure 2.5 (c)) assume that the DRA is mounted on an infinite ground plane. For practical applications, DRAs are mounted on finite ground planes, which will have an effect on the radiation patterns due to diffraction from the edges. These effects will be considered in the next section.

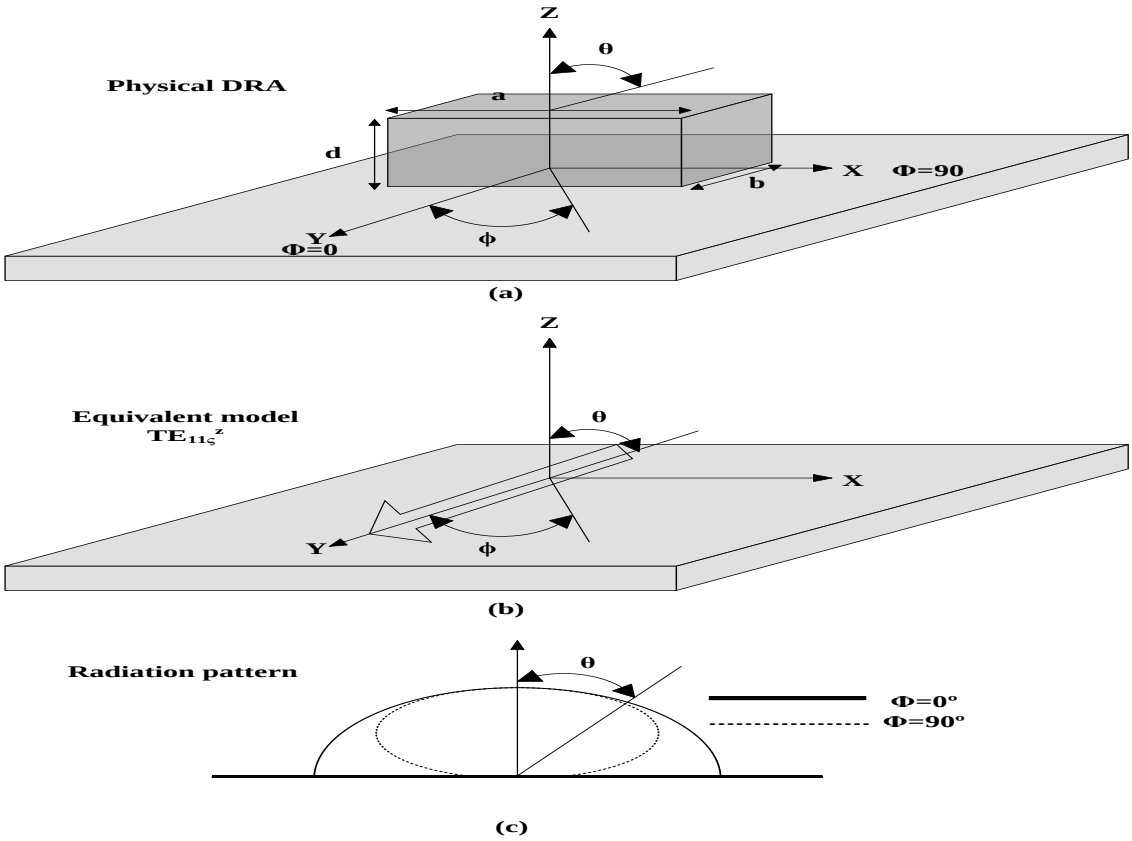

Figure 2.5: The radiation model of rectangular DRA (Luk and Leung, 2002)

2.1.3.6 Radiation Efficiency of a Rectangular DRA

There are several methods for estimating the radiation efficiency of antennas. For physically small antennas a useful technique is the Wheeler cap method (Wheeler,

1959). The total power (P) can be divided into two components: radiated power (P_{rad}) and power dissipated as heat (P_{dis}):

$$P = P_{rad} + P_{dis} \tag{2.18}$$

The Q-factor of the antenna can thus be decomposed into a radiation Q-factor (Q_{rad}) and a dissipation Q-factor (Q_{dis}):

$$\frac{1}{Q_o} = \frac{P_{rad} + P_{dis}}{\omega W} = \frac{1}{Q_{rad}} + \frac{1}{Q_{dis}} \tag{2.19}$$

The radiation efficiency (η) of the antenna is the ratio of the radiated power (P_{rad}) to the total power which can also be expressed in terms of Q-factors as:

$$\eta = \frac{P_{rad}}{P_{rad} + P_{dis}} = 1 - \frac{Q_o}{Q_{dis}} \tag{2.20}$$

2.1.3.7 Rectangular Dielectric Resonator Dimensions

Figure 2.6 shows a rectangular DR fed by a microstrip coupling system (Ittipiboon et al., 1993). When the length of the slot is along the dimension d the TE^{Z}_{111} mode of the resonator is excited, in this mode the resonator radiated as a Z-directed magnitude dipole. The resonating frequency in the mode TE^{Z}_{111} in this antenna can be determined using the equations.

$$f_0 = \frac{c}{2\pi\sqrt{\varepsilon_r}}\sqrt{k_x^2 + k_y^2 + k_z^2} \tag{2.21}$$

where $k_x = \pi/a$, $k_y = \pi/2b$, $k_z \le \pi/d$

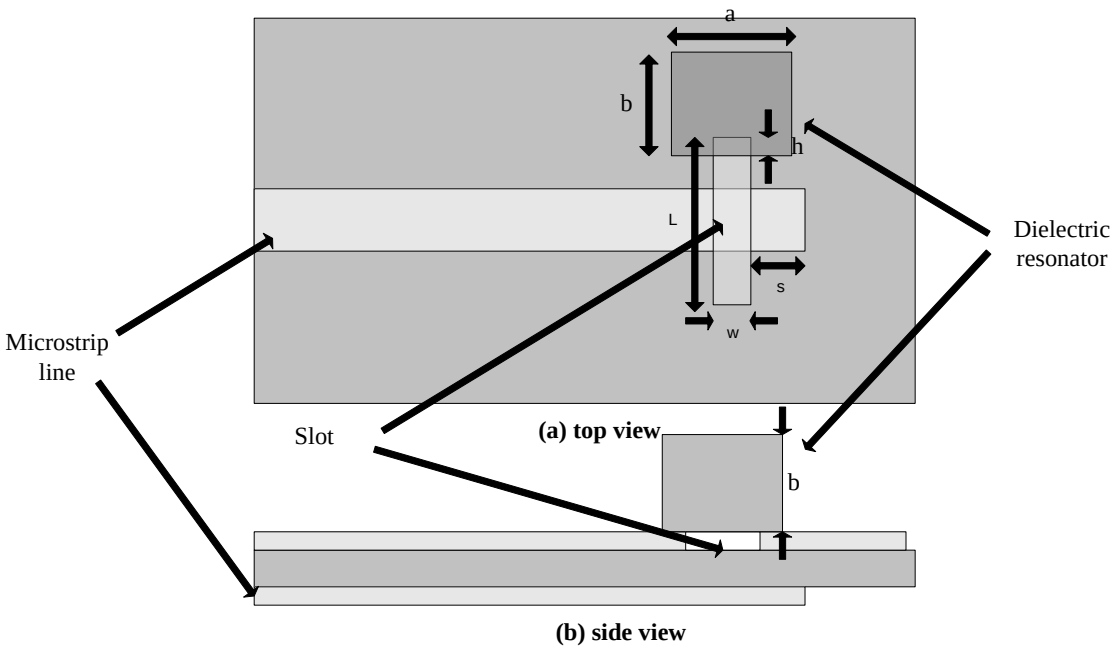

Figure 2.6: Microstrip slot coupled rectangular dielectric resonator antenna (Ittipiboon et al., 1993)

2.1.4 Substrate Parameters Effects on Antenna

The bandwidth of microstrip antennas increases by increasing the substrate height (James and Hall, 1989). Half power bandwidth is given as (Alexopoulos et al., 1982):

$$BW = \frac{2G}{\omega_0 \left.\frac{dB}{d\omega}\right|_{\omega_0}} \tag{2.22}$$

where

$Y = G + jB$ is the input impedance at resonant frequency ω_0.